



Cite this: *New J. Chem.*, 2018, 42, 8661

Influence of ancillary ligands on the photophysical properties of cyclometalated organoplatinum(II) complexes†

Mozhgan Samandar Sangari,^a Mohsen Golbon Haghighi,^b S. Masoud Nabavizadeh,^a Arno Pfitzner^c and Mehdi Rashidi^{*a}

Three series of cyclometalated organoplatinum(II) complexes [Pt(*p*-MeC₆H₄)(bhq)(L)], in which bhq is benzo[*h*]quinolate and L is PPh₃ (**1a**), PPh₂Me (**1b**), or PPhMe₂ (**1c**); [Pt(*p*-XC₆H₄)(bhq)(PPh₂Me)], in which X is H (**2a**), F (**2b**), ^tBu (**2c**), OMe (**2d**), or Me (**2e** = **1b**); and [Pt(bhq)X(PPh₂Me)], in which X is CF₃CO₂ (**3a**), Cl (**3b**), or I (**3c**) were synthesized and fully characterized using multinuclear (¹H and ³¹P) NMR spectroscopy and elemental analysis. Typical complexes [Pt(*p*-MeC₆H₄)(bhq)(PPhMe₂)], **1c**, [Pt(*p*-MeC₆H₄)(bhq)(PPh₂Me)], **2e**, and [Pt(bhq)Cl(PPh₂Me)], **3b**, were further characterized by single crystal X-ray crystallography. The photophysical properties of all the complexes were studied and the influence of changing the ancillary ligands and substituents on their luminescence properties were investigated and the assignments were confirmed by TD-DFT calculations.

Received 10th December 2017,
Accepted 4th April 2018

DOI: 10.1039/c7nj04888b

rsc.li/njc

1. Introduction

Significant research efforts have been focused on the photophysical properties of luminescent square planar platinum complexes. Among them, cyclometalated platinum complexes have attracted much attention as phosphorescent emitters in organic light emitting diodes (OLEDs) and luminescent probes for bioimaging.^{1–3} These applications in optical technologies are based on the strong luminescence displayed by such materials and the wide tunability of the emission properties by chemical modifications of the molecular structures.^{4,5}

In mixed-ligand [Pt(C^N)XY] complexes, the strong ligand-field influence of the aromatic carbon donor of C^N where (C^N) is the *ortho*-C-deprotonated form of 2-phenylpyridine (ppy-) and benzo[*h*]quinoline (bhq-) combined with the possibility of π -back-donation into the metallocycle yields generally high-lying MC states.^{6,7} Thus, the luminescence of these complexes originates from the lowest ligand-centered triplet state (³LC) that is perturbed by admixtures with higher lying metal-to-ligand charge-transfer singlet and triplet (^{1,3}MLCT) states.

Increasing the covalency of metal–ligand bonds eventuates to increase the MLCT character of the excited states.⁸

Unlike bis-cyclometalated Pt(II) complexes, which can be prepared by using lithiated organic ligands,⁹ the [Pt(C^N)XY] complexes, where X and Y represent monodentate and bidentate ligands with different donor and acceptor properties, are readily formed by the substitution of the labile leaving groups such as SMe₂^{6,10} and DMSO^{11,12} in the parent [Pt(C^N)Ar(S)] complexes with various X and Y reagents.

In the present paper, we investigated the photophysical properties of three series of cyclometalated organoplatinum(II) complexes, by modifying different kinds of ancillary ligands and changing the substituents on them and the effects of each part on their luminescence properties were studied. For better understanding and interpretation of the relationship between luminescence properties and structural details, DFT and TD-DFT calculations were employed on electronic transitions and geometrical structures.

2. Experimental

2.1. General remarks

The NMR spectra were recorded on a Bruker Avance DPX 250 MHz spectrometer (¹H), a Bruker Avance DRX 400 MHz spectrometer (¹H and ³¹P), or a Bruker Avance DRX 500 MHz spectrometer (¹H and ³¹P). The operating frequencies and references, respectively, are shown in parentheses as follows: ¹H (250 MHz, 400 MHz, or 500 MHz, TMS), ³¹P (162 MHz or 202 MHz, 85% H₃PO₄). The chemical shifts and coupling

^a Professor Rashidi Laboratory of Organometallic Chemistry, Department of Chemistry, College of Sciences, Shiraz University, Shiraz 71467-13565, Iran

^b Department of Chemistry, Shahid Beheshti University, Evin, Tehran 19839-69411, Iran. E-mail: m_golbon@sbu.ac.ir

^c Institut für Anorganische Chemie, Universität Regensburg, Universitätsstrasse 31, Regensburg D-93053, Germany

† Electronic supplementary information (ESI) available. CCDC 1513088–1513090. For ESI and crystallographic data in CIF or other electronic format see DOI: 10.1039/c7nj04888b

constants are in ppm and Hz, respectively. The microanalyses were performed using a Thermofinigan Flash EA-1112 CHNSO rapid elemental analyzer. The UV-vis absorption spectra were carried out in a PerkinElmer Lambda 25 spectrophotometer in a cuvette with a 1 cm and/or 1 mm path length. The emission spectra were obtained on a PerkinElmer LS45 fluorescence spectrometer with the lifetimes measured in phosphorimeter mode. Absolute measurements of the photoluminescence quantum yield at ambient temperature under Ar were performed with a C9920202 (Hamamatsu Photonics) system equipped with a Spectralon[®] integrating sphere. The precursors [Pt(*p*-MeC₆H₄)(bhq)(SMe₂)], in which bhq is benzo[*h*]quinoline,¹³ [Pt(bhq)(CF₃CO₂)(SMe₂)],¹⁴ [Pt(bhq)Cl(DMSO)],¹⁵ and *cis*-[Pt(*p*-XC₆H₄)₂(SMe₂)₂],¹⁶ were synthesized similar to literature methods. The complex [Pt(bhq)I(DMSO)] was prepared similar to ref. 17 by the reaction of [Pt(bhq)Cl(DMSO)] with 3 equiv. NaI in acetone. After stirring overnight, the solvent was evaporated and the residue was extracted by dichloromethane. The product was obtained by evaporation of the dichloromethane solution under reduced pressure and then washing the residue with diethyl ether (2 × 2 ml). Yield 82%; C₁₅H₁₄INOSPt: calcd C, 31.1; H, 2.4; N, 2.4; found: C, 30.5; H, 2.2; N, 2.3. NMR data in CDCl₃: δ (¹H) = 4.00 (s, ³J_{PH} = 24.6 Hz, DMSO); aromatic protons: 6.8–9.5.

2.2. Synthesis of the complexes

[Pt(*p*-MeC₆H₄)(bhq)(PPh₃)], **1a**. *cis*-[Pt(*p*-MeC₆H₄)₂(SMe₂)₂] (150 mg, 0.3 mmol) was dissolved in acetone (30 mL) and benzo[*h*]quinoline (55 mg, 0.3 mmol) was added. The reaction mixture was refluxed for 12 h. After cooling, 1.05 equiv. PPh₃ was added to the mixture and stirred at RT for 2 h. The solvent was removed under reduced pressure and the residue was washed with cold diethyl ether (2 × 2 ml). The yellowish green solid was dried under vacuum. Yield: 168 mg, 77%. Anal. calcd for C₃₈H₃₀NPt: C, 62.8, H, 4.2, N, 1.9; found: C, 62.3, H, 4.0, N, 2.0. NMR data in CDCl₃: δ (¹H) = 2.14 (s, 3H, CH₃ of *p*-MeC₆H₄), aromatic protons: 6.4–8.2; δ (³¹P) = 30.6 (s, ¹J_{PPt} = 2107 Hz, *P trans* to C of bhq in PPh₃).

The following complexes were prepared similarly by using the appropriate starting complexes *cis*-[Pt(*p*-XC₆H₄)₂(SMe₂)₂] and the related phosphine ligands PPh₂Me or PPhMe₂.

[Pt(*p*-MeC₆H₄)(bhq)(PPh₂Me)], **1b** (= **2e**). Yield: 82%. Anal. calcd for C₃₃H₂₈NPt: C, 59.6, H, 4.3, N, 2.1; found: C, 59.4, H, 5.0, N, 1.9. NMR data in CDCl₃: δ (¹H) = 1.49 (d, ²J_{PH} = 8.9 Hz, ³J_{PH} = 27.0 Hz, 3H, CH₃ of PPh₂Me), 2.28 (s, 3H, CH₃ of *p*-MeC₆H₄), aromatic protons: 6.8–8.2; δ (³¹P) = 13.5 (s, ¹J_{PPt} = 2061 Hz, *P trans* to C of bhq in PPh₂Me).

[Pt(*p*-MeC₆H₄)(bhq)(PPhMe₂)], **1c**. Yield: 71%. Anal. calcd for C₂₈H₂₆NPt: C, 55.8, H, 4.4, N, 2.3; found: C, 56.2, H, 4.2, N, 2.7. NMR data in CDCl₃: δ (¹H) = 1.54 (d, ²J_{PH} = 8.2 Hz, ³J_{PH} = 23.5 Hz, 6H, CH₃ of PPhMe₂), 2.32 (s, 3H, CH₃ of *p*-MeC₆H₄), aromatic protons: 6.9–8.2; δ (³¹P) = −1.3 (s, ¹J_{PPt} = 2010 Hz, *P trans* to C of bhq in PPhMe₂).

[Pt(C₆H₅)(bhq)(PPh₂Me)], **2a**. Yield: 85%. Anal. calcd for C₃₂H₂₆NPt: C, 59.1, H, 4.0, N, 2.2; found: C, 58.4, H, 4.3, N, 2.5. NMR data in CDCl₃: δ (¹H) = 1.50 (d, ²J_{PH} = 8.7 Hz, ³J_{PH} = 27.0 Hz, 3H, CH₃ of PPh₂Me), aromatic protons: 6.9–8.2; δ (³¹P) = 13.5 (s, ¹J_{PPt} = 2060 Hz, *P trans* to C of bhq in PPh₂Me).

[Pt(*p*-FC₆H₄)(bhq)(PPh₂Me)], **2b**. Yield: 61%. Anal. calcd for C₃₂H₂₅NFPt: C, 57.5, H, 3.7, N, 2.1; found: C, 56.6, H, 3.1, N, 1.7. NMR data in CDCl₃: δ (¹H) = 2.51 (d, ²J_{PH} = 10.9 Hz, ³J_{PH} = 36.1 Hz, 3H, CH₃ of PPh₂Me), 10.33 (br. t, ³J_{HH} ≈ ⁴J_{PH} = 4.7 Hz, 1H, H⁸ of bhq), other aromatic protons: 6.7–8.4; δ (³¹P) = 14.8 (s, ¹J_{PPt} = 2197 Hz, *P trans* to C of bhq in PPh₂Me).

[Pt(*p*-^{*t*}BuC₆H₄)(bhq)(PPh₂Me)], **2c**. Yield: 68%. Anal. calcd for C₃₆H₃₄NPt: C, 61.2, H, 4.9, N, 1.98; found: C, 60.6, H, 4.6, N, 2.1. NMR data in CDCl₃: δ (¹H) = 1.31 (s, 9H, C(CH₃)₃ of *p*-^{*t*}BuC₆H₄), 1.47 (d, ²J_{PH} = 8.7 Hz, ³J_{PH} = 26.3 Hz, 3H, CH₃ of PPh₂Me), aromatic protons: 6.9–8.2; δ (³¹P) = 14.0 (s, ¹J_{PPt} = 2063 Hz, *P trans* to C of bhq in PPh₂Me).

[Pt(*p*-MeOC₆H₄)(bhq)(PPh₂Me)], **2d**. Yield: 79%. Anal. calcd for C₃₂H₂₈NOPt: C, 58.2, H, 4.1, N, 2.1; found: C, 58.0, H, 4.3, N, 1.9. NMR data in CDCl₃: δ (¹H) = 1.49 (d, ²J_{PH} = 8.7 Hz, ³J_{PH} = 26.5 Hz, 3H, CH₃ of PPh₂Me), 3.79 (s, 3H, CH₃ of *p*-MeOC₆H₄), aromatic protons: 6.6–8.2; δ (³¹P) = 13.6 (s, ¹J_{PPt} = 2044 Hz, *P trans* to C of bhq in PPh₂Me).

[Pt(bhq)(CF₃CO₂)(PPh₂Me)], **3a**. To a solution of [Pt(bhq)(CF₃CO₂)(SMe₂)] (55 mg, 0.1 mmol) in acetone (15 ml) was added PPh₂Me (19 μl, 0.1 mmol). The mixture was stirred at RT for 2 h. The solvent was removed under reduced pressure and the residue was washed with cold diethyl ether (2 × 2 ml). The yellow solid was dried under vacuum. Yield: 52 mg, 76%. Anal. calcd for C₂₈H₂₁NO₂F₃PPt: C, 49.0, H, 3.0, N, 2.0; found: C, 48.6, H, 2.5, N, 2.3. NMR data in CDCl₃: δ (¹H) = 2.34 (d, ²J_{PH} = 10.6 Hz, ³J_{PH} = 40.4 Hz, 3H, CH₃ of PPh₂Me), 6.92 (dd, ³J_{HH} = 7.2 Hz, ⁴J_{PH} = 2.4 Hz, ³J_{PH} ≈ 53 Hz, 1H, H¹ of bhq), 8.82 (br. t, ³J_{HH} ≈ ⁴J_{PH} = 4.5 Hz, 1H, H⁸ of bhq), other aromatic protons: 7.0–8.0; δ (³¹P) = 4.9 (s, ¹J_{PPt} = 4317 Hz, *P trans* to N of bhq in PPh₂Me).

[Pt(bhq)Cl(PPh₂Me)], **3b**. This compound was prepared similarly to complex **3a** by using [Pt(bhq)Cl(DMSO)]. Yield: 82%. Anal. calcd for C₂₆H₂₁NPClPt: C, 51.3, H, 3.5, N, 2.3; found: C, 50.7, H, 3.1, N, 2.6. NMR data in CDCl₃: δ (¹H) = 2.38 (d, ²J_{PH} = 11.0 Hz, ³J_{PH} = 33.9 Hz, 3H, CH₃ of PPh₂Me), 6.85 (dd, ³J_{HH} = 7.2 Hz, ⁴J_{PH} = 2.6 Hz, ³J_{PH} ≈ 56 Hz, 1H, H¹ of bhq), 10.05 (br. t, ³J_{HH} ≈ ⁴J_{PH} = 4.1 Hz, 1H, H⁸ of bhq), other aromatic protons: 6.9–8.4; δ (³¹P) = 4.9 (s, ¹J_{PPt} = 4252 Hz, *P trans* to N of bhq in PPh₂Me).

[Pt(bhq)I(PPh₂Me)], **3c**. Compound **3c** was prepared similarly to complex **3a** by using [Pt(bhq)I(DMSO)]. Yield: 66%. Anal. calcd for C₂₆H₂₁NOPt: C, 44.6, H, 3.0, N, 2.0; found: C, 44.1, H, 2.7, N, 2.1. NMR data in CDCl₃: δ (¹H) = 2.69 (d, ²J_{PH} = 10.6 Hz, ³J_{PH} = 38.9 Hz, 3H, CH₃ of PPh₂Me), 6.85 (dd, ³J_{HH} = 7.3 Hz, ⁴J_{PH} = 3.8 Hz, ³J_{PH} ≈ 57 Hz, 1H, H¹ of bhq), 10.72 (br. t, ³J_{HH} ≈ ⁴J_{PH} = 4.8 Hz, 1H, H⁸ of bhq), other aromatic protons: 6.9–8.4; δ (³¹P) = 3.7 (s, ¹J_{PPt} = 4184 Hz, *P trans* to N of bhq in PPh₂Me).

2.3. Computational details

Density functional calculations were performed with the program suite Gaussian 03¹⁸ using the B3LYP level of theory. The LANL2DZ basis set¹⁹ was chosen to describe Pt. The 6-31G(d) basis set was used for all other atoms. The geometries of the complexes under discussion were fully optimized by employing density functional theory without imposing any symmetry constraints. To evaluate

Table 1 Crystal data and structure refinements for **1c**, **2e** and **3b** complexes

	1c	2e	3b
Empirical formula	C ₂₈ H ₂₆ NPt	C ₃₃ H ₂₈ NPt	C ₂₆ H ₂₁ ClNPt
Formula weight	602.56	664.62	608.95
Temperature	296.17(10) K	123.0 K	293.0 K
Wavelength	1.54184 Å	0.71073 Å	1.54184 Å
Crystal system	Monoclinic	Triclinic	Monoclinic
Space group	P2 ₁ /c (no. 14)	P $\bar{1}$ (no. 2)	P2 ₁ /c (no. 14)
Unit cell dimensions	<i>a</i> = 10.8604(3) Å <i>b</i> = 9.7288(3) Å <i>c</i> = 21.8042(6) Å β = 92.492(2)°	<i>a</i> = 10.8827(3) Å <i>b</i> = 11.0853(4) Å <i>c</i> = 11.3916(2) Å α = 95.334(2)° β = 100.076(2)° γ = 99.549(2)°	<i>a</i> = 16.0265(5) Å <i>b</i> = 18.9031(5) Å <i>c</i> = 14.5969(4) Å β = 107.211(3)°
Volume	2301.62(11) Å ³	1323.75(7) Å ³	4224.1(2) Å ³
Z	4	2	8
Absorption coefficient	$\rho(\text{CuK}\alpha) = 12.163 \text{ mm}^{-1}$	$\rho(\text{MoK}\alpha) = 5.383 \text{ mm}^{-1}$	$\rho(\text{CuK}\alpha) = 14.402 \text{ mm}^{-1}$
<i>F</i> (000)	1176	652	2352
Theta range for data collection	4.058 to 66.780°	2.960 to 26.370°	3.69 to 73.28°
Reflections collected	20515	14350	20764
Independent reflections	4034 [<i>R</i> (int) = 0.0291]	5361 [<i>R</i> (int) = 0.0282]	8214 [<i>R</i> (int) = 0.0256]
Observed reflections	3631	5049	7411
Completeness to theta max	98.8%	99.0%	99.3%
Absorption correction	Gaussian	Gaussian	Gaussian
<i>T</i> _{min} / <i>T</i> _{max}	0.559/0.705	0.466/0.718	0.248/0.407
Refinement method	Full-matrix least-squares on <i>F</i> ²	Full-matrix least-squares on <i>F</i> ²	Full-matrix least-squares on <i>F</i> ²
Data/restraints/parameters	4034/0/280	5357/0/325	8214/0/541
Goodness-of-fit on <i>F</i> ²	1.20	1.33	1.10
Final <i>R</i> indices [<i>I</i> > 3σ(<i>I</i>)]	<i>R</i> ₁ = 0.0165, <i>wR</i> ₂ = 0.0399	<i>R</i> ₁ = 0.0177, <i>wR</i> ₂ = 0.0449	<i>R</i> ₁ = 0.0186, <i>wR</i> ₂ = 0.0438
<i>R</i> indices (all data)	<i>R</i> ₁ = 0.0197, <i>wR</i> ₂ = 0.0414	<i>R</i> ₁ = 0.0208, <i>wR</i> ₂ = 0.0459	<i>R</i> ₁ = 0.0223, <i>wR</i> ₂ = 0.0460
Largest diff. peak and hole	0.63 and −0.50 e Å ^{−3}	0.59 and −0.60 e Å ^{−3}	0.35 and −0.59 e Å ^{−3}

and ensure the optimized structures of the molecules, frequency calculations were carried out using analytical second derivatives. In all cases only real frequencies were obtained for the optimized structures. The solvent effects of CH₂Cl₂ were taken into account using the PCM model.^{20,21} Computations of electronic absorption spectra using time-dependent DFT (TD-DFT) were carried out at the same level. The composition of the molecular orbitals and theoretical absorption spectra were plotted using the Chemissian program.^{22,23} The NBO analyses were carried out on the stationary points using the NBO 3.1 program²⁴ as implemented in the Gaussian 03 program suite.

2.4. X-ray structure determination

Single crystals of **1c**, **2e** and **3b** were obtained by slow evaporation from a CH₂Cl₂ solution. X-ray diffraction data of suitable single-crystals of **1c**, **2e** and **3b** were collected at 296 K (**1c**) and 123 K (**2e** and **3b**) by the ω -scan technique on Agilent Technologies four-circle diffractometers: **2e** on an Xcalibur with an Eos CCD detector and monochromated MoK α radiation (λ = 0.71073 Å), and **1c** and **3b** on a SuperNova with an Atlas CCD detector, equipped with a Nova microfocus Cu-K α radiation source (λ = 1.54184 Å). The obtained diffraction data were corrected for Lorentz- and polarization effects and corrected by analytical absorption corrections using the CrysAlisPro software package.²⁵ The crystals were fixed on a microloop in mineral oil and the crystal structures of the title compounds were solved with Superflip²⁶ in the JANA2006 program package.²⁷ The positions of all the non-hydrogen atoms were found from structure solutions and were then subsequently refined with anisotropic

displacement parameters. H atoms were inserted by geometrical considerations and refined by the riding model with fixed bond distances and a displacement parameter derived from that of the central atom.

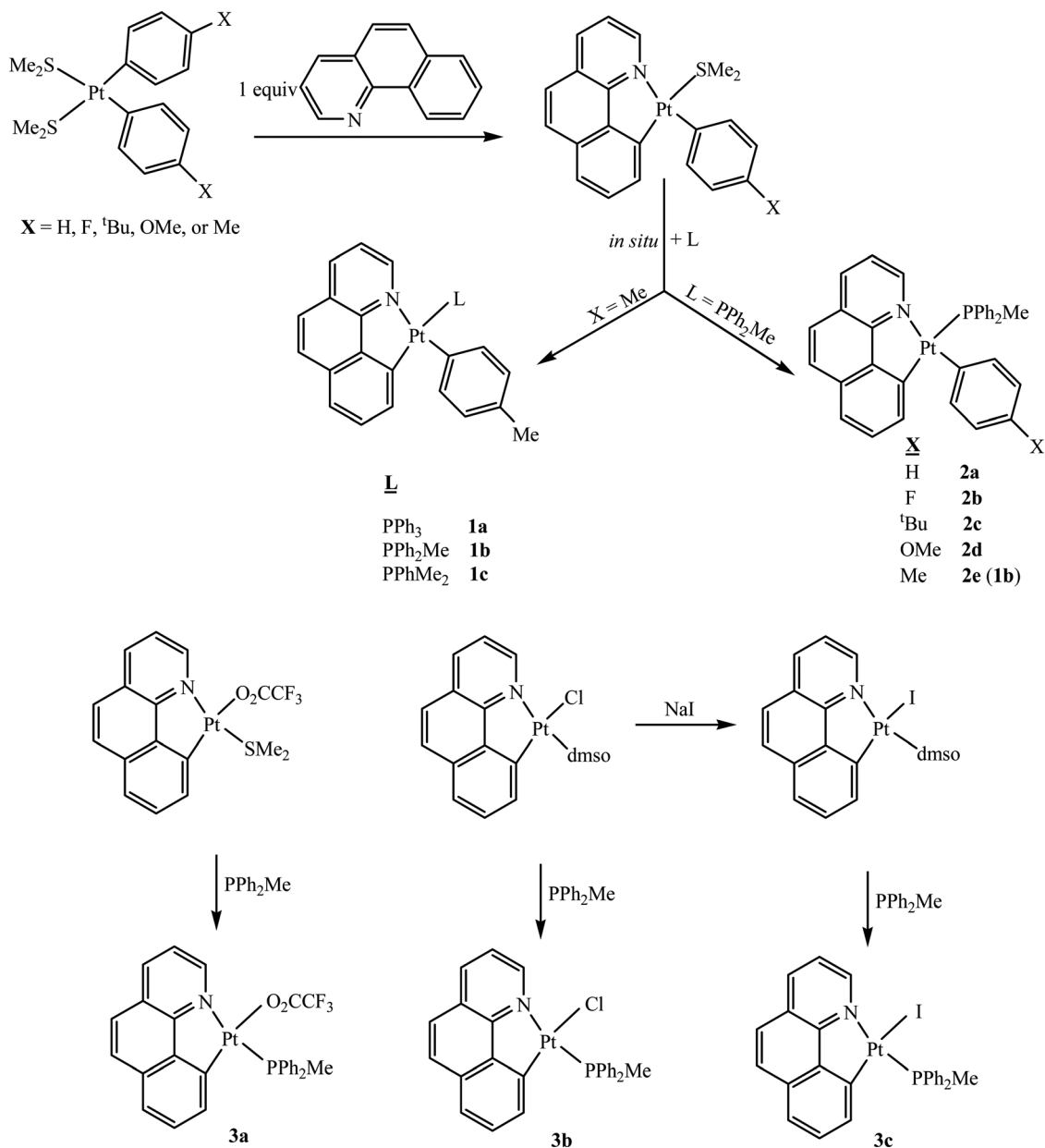
It has to be noted that the crystal structure of **3b** contains two crystallographically independent molecules which differ only slightly in their geometrical parameters. However, no hint of a superstructure was found (Table 1).

Atomic coordinates and displacement parameters are deposited with the CCDC 1513089(**1c**), 1513090(**2e**) and 1513088(**3b**) contain the supplementary crystallographic data for this paper.[†]

3. Results and discussion

3.1. Synthesis

The synthetic routes used in the present work are depicted in Scheme 1. The known starting complexes [Pt(*p*-MeC₆H₄)(bhq)(SMe₂)], in which bhq is deprotonated benzo[*h*]quinoline,²⁸ [Pt(bhq)(CF₃CO₂)(SMe₂)] and [Pt(bhq)Cl(DMSO)],¹⁵ have all been prepared as reported previously. Also as is described in Scheme 1, the cyclometalated organoplatinum(II) complexes [Pt(*p*-MeC₆H₄)(bhq)(L)], in which L is PPh₃ (**1a**), PPh₂Me (**1b**), or PPhMe₂ (**1c**), and [Pt(*p*-XC₆H₄)(bhq)(PPh₂Me)], in which X is H (**2a**), F (**2b**), ^tBu (**2c**), OMe (**2d**), or Me (**2e** = **1b**), were synthesized using the known method²⁹ by reaction of the complex [Pt(*p*-XC₆H₄)₂(SMe₂)₂] with 1 equiv. of bhq in acetone, followed by the reaction of the resulting product [Pt(*p*-XC₆H₄)(bhq)(SMe₂)] with 1 equiv. of the related phosphine (PPh₃, PPh₂Me, or PPhMe₂). Besides, the complexes [Pt(bhq)X(PPh₂Me)], in which X is



Scheme 1 Synthetic routes for the preparation of the three series of cyclometalated organoplatinum(II) complexes.

CF₃CO₂ (**3a**), Cl (**3b**), or I (**3c**), were synthesized by the reaction of the known complexes [PtX(bhq)(S)], in which S is dimethyl sulfide (SMe₂) or dimethylsulphoxide (DMSO), with 1 equiv. of PPh₂Me in acetone (see Scheme 1).

3.2. Characterization

The structures of the cyclometalated organoplatinum(II) complexes [Pt(*p*-MeC₆H₄)(bhq)(L)], **1**, [Pt(*p*-XC₆H₄)(bhq)(PPh₂Me)], **2**, and [Pt(bhq)X(PPh₂Me)], **3**, in solution were characterized using ¹H and ³¹P NMR spectroscopy. Typical spectra are shown in Fig. 1 (¹H NMR spectra) and Fig. 2 (³¹P NMR spectra) for the cyclometalated organoplatinum(II) complexes [Pt(*p*-MeC₆H₄)(bhq)(PPhMe₂)], **1c**, [Pt(*p*-MeC₆H₄)(bhq)(PPh₂Me)], **2e**, and [Pt(bhq)(CF₃CO₂)(PPh₂Me)], **3a**. In the ¹H NMR spectra of

complexes **1c** and **2e** a doublet signal, accompanied by Pt satellites, was observed for the Me groups of the phosphine ligands, being *trans* to the C ligating atom of the bhq chelate, at $\delta = 1.54$ (with $^2J_{\text{PH}} = 8.2$ Hz and $^3J_{\text{PH}} = 23.5$ Hz) and $\delta = 1.49$ (with $^2J_{\text{PH}} = 8.9$ Hz and $^3J_{\text{PH}} = 27.0$ Hz), respectively; a similar pattern was also observed for **3a** at $\delta = 2.34$ with higher values for $^2J_{\text{PH}}$ (10.6 Hz) and $^3J_{\text{PH}}$ (40.4 Hz), as compared with the corresponding values for **1c** and **2e**. This confirms that in **3a**, the phosphine ligand is situated *trans* to the N ligating atom of the bhq chelate as compared with **1c** and **2e** in which the phosphine ligands are located *trans* to the C ligating atom of the bhq chelate, that having a much higher *trans* influence than the N atom. Consistently, in the ³¹P NMR spectra of each of the complexes **1c** or **2e** (see Fig. 2), a singlet signal accompanied by

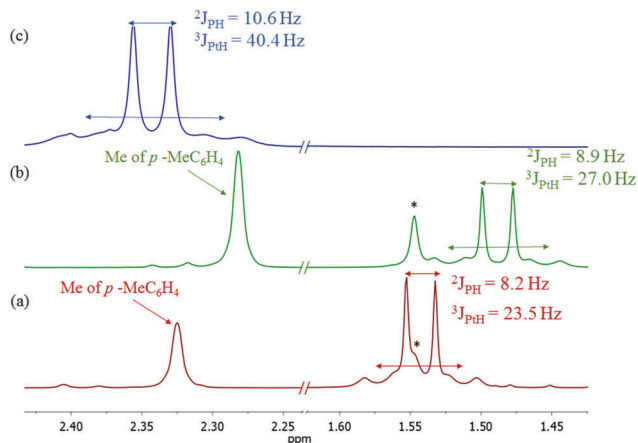


Fig. 1 ^1H NMR spectra in the Me regions of $[\text{Pt}(p\text{-MeC}_6\text{H}_4)(\text{bhq})(\text{PPh}_2\text{Me})]$, **1c** (a), $[\text{Pt}(p\text{-MeC}_6\text{H}_4)(\text{bhq})(\text{PPh}_2\text{Me})]$, **2e** (b), and $[\text{Pt}(\text{bhq})(\text{CF}_3\text{CO}_2)(\text{PPh}_2\text{Me})]$, **3a** (c). Trace water impurities of NMR solvent are shown by *.

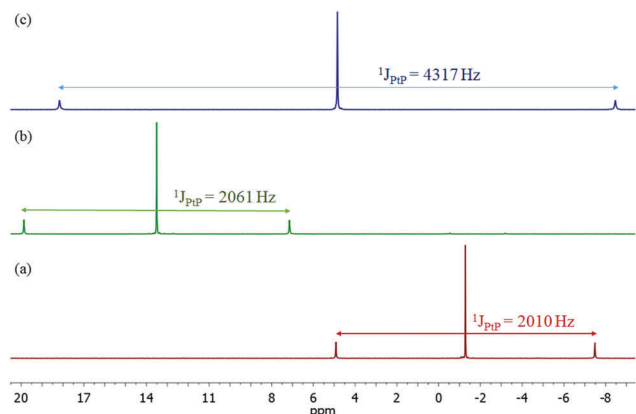


Fig. 2 ^{31}P NMR spectra of $[\text{Pt}(p\text{-MeC}_6\text{H}_4)(\text{bhq})(\text{PPh}_2\text{Me})]$, **1c** (a), $[\text{Pt}(p\text{-MeC}_6\text{H}_4)(\text{bhq})(\text{PPh}_2\text{Me})]$, **2e** (b), and $[\text{Pt}(\text{bhq})(\text{CF}_3\text{CO}_2)(\text{PPh}_2\text{Me})]$, **3a** (c).

Pt satellites is observed for the phosphine ligand (being *trans* to C) at $\delta = -1.3$ (with $^1J_{\text{PTP}} = 2010$ Hz) or $\delta = 13.5$ (with $^1J_{\text{PTP}} = 2061$ Hz), respectively. However the corresponding signal for **3a**, with the phosphine being *trans* to the N ligating atom, was observed at $\delta = 4.9$ with a much higher $^1J_{\text{PTP}}$ value of 4317 Hz.

The structures of typical cyclometalated organoplatinum(II) complexes **1c**, **2e** and **3b** were further confirmed by X-ray crystallography determination. The ellipsoid representation of complexes and the packing of molecules through different kinds of intermolecular interactions are also illustrated in Fig. 3 (**1c** and **2e**) and Fig. 4 (**3b**) and selected geometric parameters are listed. Suitable crystals were grown through slow diffusion of *n*-hexane into the CH_2Cl_2 solution of each complex. All complexes exhibit a distorted square planar geometry around the Pt center in which the chelating C \cdots N bite angles (N1-Pt1-C1) are 80.42, 80.13 and 81.02 for complexes **1c**, **2e** and **3b**, respectively. They are significantly smaller than 90° which implies that the chelates are probably under strain. In complex **1c**, the *p*-MeC $_6$ H $_4$ ligand lies orthogonal at $90.2(2)^\circ$ to the plane of the platinum center.

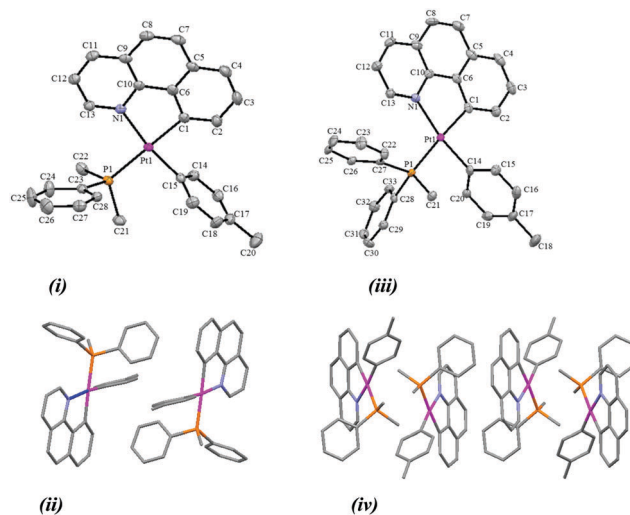


Fig. 3 (i) Anisotropic representation and (ii) packing of molecules for the complex $[(p\text{-MeC}_6\text{H}_4)(\text{bhq})\text{Pt}(\text{PPh}_2\text{Me})]$, **1c**. Ellipsoids are shown at the 50% probability level. Selected geometrical parameters (\AA , $^\circ$): Pt1–C15 2.013(0); Pt1–C1 2.041(1); Pt1–N1 2.145(0); Pt1–P1 2.294(1); C15–Pt1–C1 90.54(0); C15–Pt1–N1 170.91(1); C1–Pt1–N1 80.42(0); C15–Pt1–P1 90.45(0); C1–Pt1–P1 176.38(0); N1–Pt1–P1 98.63(0). (iii) Anisotropic representation and (iv) packing of molecules through C–H \cdots Pt intermolecular hydrogen bonding for the complex $[(p\text{-MeC}_6\text{H}_4)(\text{bhq})\text{Pt}(\text{PPh}_2\text{Me})]$, **2e**. Ellipsoids are shown at the 50% probability level. Selected geometrical parameters (\AA , $^\circ$): Pt1–C1 2.051(2); Pt1–N1 2.136(2); Pt1–C14 2.016(2); Pt1–P1 2.302(2); C1–Pt1–C14 91.34(0); C1–Pt1–N1 80.16(0); C14–Pt1–P1 85.51(0); N1–Pt1–P1 102.97(0); C1–Pt1–P1 176.84(0); N1–Pt1–C14 170.65(0). Intramolecular and intermolecular hydrogen bonds (\AA , $^\circ$): D–H \cdots A, for C23–H23 \cdots Pt1, $d(\text{D–H}) = 0.94$, $d(\text{H}\cdots\text{A}) = 2.68$, $d(\text{D}\cdots\text{A}) = 3.59$, $\angle(\text{DHA}) = 161.9$.

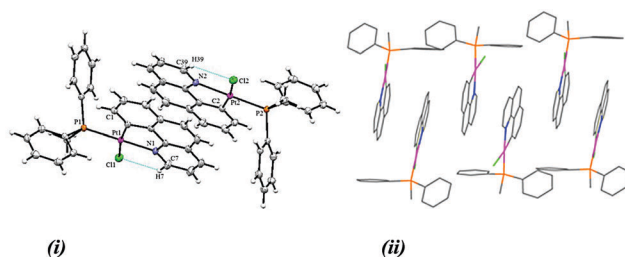


Fig. 4 (i) ORTEP anisotropic drawing of two independent molecules and (ii) packing of molecules of the complex **3b**. Ellipsoids are shown at the 50% probability level. Selected bond lengths (\AA) and angles ($^\circ$): Pt1–P1 2.2243(7), Pt1–C11 2.3973(7), Pt1–N1 2.099(2), Pt1–C1 2.013(3), Pt2–P2 2.2242(7), Pt2–C12 2.3937(6), Pt2–N2 2.106(2), Pt2–C2 2.014(3); N1–Pt1–C1 81.02(10), N1–Pt1–C11 90.82(7), N1–Pt1–P1 176.19(7), C1–Pt1–P1 95.86(8), C1–Pt1–C11 170.87(8), P1–Pt1–C11 92.44(2), N2–Pt2–C2 81.23(11), N2–Pt2–C12 90.60(7), N2–Pt2–P2 176.74(7), C2–Pt2–C12 171.30(8), C2–Pt2–P2 96.06(8), C12–Pt2–P2 92.20(2). Intramolecular hydrogen bonds (\AA , $^\circ$): D–H \cdots A, for C7–H7 \cdots C11, $d(\text{D–H}) = 0.93$, $d(\text{H}\cdots\text{A}) = 2.57$, $d(\text{D}\cdots\text{A}) = 3.24$, $\angle(\text{DHA}) = 129.0$; for C39–H39 \cdots C12, $d(\text{D–H}) = 0.92$, $d(\text{H}\cdots\text{A}) = 2.62$, $d(\text{D}\cdots\text{A}) = 3.25$, $\angle(\text{DHA}) = 125.8$.

Complex **3b** was crystallized in the monoclinic crystal system in the space group of $P2_1/c$. Two crystallographically different but chemically identical complexes are located in the asymmetric unit. Bond lengths and angles are slightly different for the independent molecules. No hints of higher symmetry

Table 2 Electronic absorption data for the studied complexes in CH₂Cl₂ solution (ca. 3×10^{-5} M) at 298 K

	λ_{max} , nm ($\epsilon \times 10^{-3}$ M ⁻¹ cm ⁻¹)
1a	290 (18.2), 324 (11.2), 379 (4.2), 403 (2.5)
1b (2e)	261 (32.7), 290 (16.4), 309 (14.3), 325 (10.7), 378 (4.3), 404 (2.4)
1c	260 (33.97), 290 (16.8), 324 (10.7), 376 (4.3), 405 (2.4)
2a	259 (33.0), 285 (22.2), 325 (7.1), 373 (2.8), 408 (1.3)
2b	260 (31.7), 305 (13.9), 328 (8.3), 414 (2.99)
2c	260 (36.5), 290 (24.3), 326 (7.5), 376 (3.2), 413 (1.4)
2d	258 (37.4), 292 (22.4), 327 (7.6), 375 (3.4), 410 (2.0)
3a	253 (40.0), 287 (19.0), 304 (16.8), 325 (7.9), 390 (3.0), 408 (3.2)
3b	258 (35.0), 305 (14.7), 394 (3.1), 413 (3.4)
3c	264 (34.6), 310 (12.5), 344 (3.6), 417 (2.0)

were found. As expected, the bhq ligand in complex **3b** binds to the Pt^{II} metal center *via* two N and C atoms. The angles around the Pt center deviate significantly from 90°, *i.e.* the (bhq) bite angles, C1–Pt1–N1 and C2–Pt2–N2 are reduced to 81.02(10)° and 81.23(11)°, respectively, implying that the chelate is probably under strain, whereas the angles formed by the chlorine ligand *trans* to C with the P atom of PPh₂Me, *i.e.* P1–Pt1–Cl1 and P2–Pt2–Cl2, are increased to 92.44(2)° and 92.20(2)°, respectively. The shortest intermolecular π -stacking distance of the bhq groups for complex **3b** is ≈ 3.6 Å (Fig. 4). Molecules of this complex assemble to give a supramolecular polymer structure through π -stacking between parallel bhq groups, as shown in Fig. 4ii, while in the adjacent molecules of complexes **1c** and **2e** secondary bonding occurs through a

series of edge-to-face and vertex-to-face aryl...aryl attractions (Fig. 3ii and iv).

3.3. Electronic absorption spectra

The UV-vis absorption spectra of the studied cyclometalated organoplatinum(II) complexes were obtained in CH₂Cl₂ solutions at 298 K; the consequent data are summarized in Table 2 and the spectra are shown in Fig. 5. All complexes exhibit intense ($\epsilon > 10^4$ M⁻¹ cm⁻¹) high-energy bands (λ range: 250–350 nm) as well as significantly less intense (ϵ : $4\text{--}4.3 \times 10^3$ M⁻¹ cm⁻¹) low-energy absorptions (λ range: 350–450 nm). These transitions are comparable to those reported for the complex [Pt(*p*-MeC₆H₄)(bhq)(SMe₂)], showing that ¹LC transitions within the bhq ligand (π – π^*) are dominating.⁶

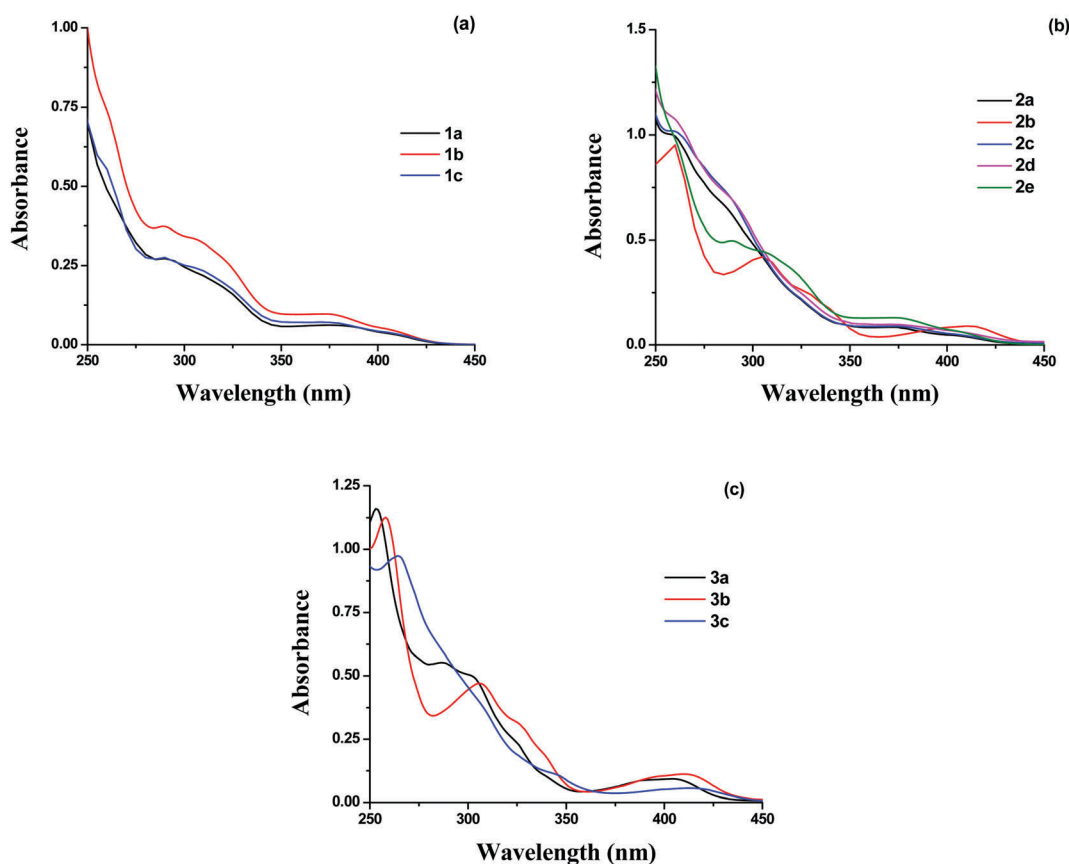
**Fig. 5** UV-visible absorption spectra, in CH₂Cl₂ at 298 K: **1** (a), **2** (b), and **3** (c).

Table 3 Emission data of the studied complexes

Complex	λ (nm)	ϕ^a	τ (μ s)	k_r^b (s^{-1})	k_{nr}^b (s^{-1})
1a	489 _{max} , 524, 567 _{sh}	5	57.34	9.0×10^2	1.7×10^4
1b (= 2e)	483 _{max} , 516, 562 _{sh} 350, 366, 385 _{sh} ^c	3	12.37	2.4×10^3	7.8×10^4
1c	485 _{max} , 513, 560 _{sh} 350, 365, 384 _{sh} ^c	11	58	1.9×10^3	1.5×10^4
2a	488 _{max} , 523, 571 _{sh}	14.6	74	2.0×10^3	1.2×10^4
2b	476 _{max} , 506, 545 _{sh}	2.1	10.6	2.0×10^3	9.2×10^4
2c	474 _{max} , 505, 548 _{sh}	2.6	17.52	1.5×10^3	5.6×10^4
2d	493 _{max} , 526, 578 _{sh}	0.8	14	6.0×10^2	7.1×10^4
3a	495 _{max} , 527, 577 _{sh}	1.3	12.18	1.1×10^3	8.1×10^4
3b	501, 532, 570 _{max}	1.8	20	9.0×10^2	4.9×10^4
3c	484, 541 _{max} , 592	1.2	15	8.0×10^2	6.6×10^4

^a In percent. ^b Radiative rate constant $k_r = \phi/\tau$, non-radiative rate constant $k_{nr} = (1 - \phi)/\tau$. ^c Measured in dichloromethane.

The lowest-energy band in either of the cyclometalated organo-platinum(II) complexes **1a–1c** comprises [LLCT; $\pi(p\text{-tol}) \rightarrow \pi^*(\text{bhq})$], [MLCT; $d\sigma(\text{Pt}) \rightarrow \pi^*(\text{bhq})$] and [LC; $\pi \rightarrow \pi^*(\text{bhq})$] transitions, showing slight dependence on the nature of the phosphine ligands. The lowest-energy slopes in the spectra of the series of complexes [Pt(*p*-XC₆H₄)(bhq)(PPh₂Me)], **2**, appear at around 408 nm; they all have [MLCT; $d\sigma(\text{Pt}) \rightarrow \pi^*(\text{bhq})$] and [LC; $\pi \rightarrow \pi^*(\text{bhq})$] transitions, with complexes **2c** and **2e** (X being an electron donor alkyl group ^tBu and Me, respectively)

having additional [LLCT; $\pi(p\text{-XC}_6\text{H}_4) \rightarrow \pi^*(\text{bhq})$] transitions. The absorption spectra of the complexes [Pt(bhq)X(PPh₂Me)], **3**, are in general similar to those found for the other series (**1** or **2**) although their maxima show minor changes with the variation of anionic ligands indicating that they arise mostly from ¹LC(bhq) transitions. The slope of the lowest-energy maxima slightly shifts to lower energies according to the π -donating ability of the X ligands by the sequence CF₃CO₂[−] (408 nm) < Cl[−] (413 nm) < I[−] (417 nm). It shows that the iodide ligand possesses a significant π -donating ability due to the presence of available (high-lying) lone pairs, and these bands originate from ligand-to-ligand charge-transfer [LLCT; $\text{I}^- \rightarrow \pi^*(\text{bhq})$], [MLCT; $d\sigma(\text{Pt}) \rightarrow \pi^*(\text{bhq})$] and [LC; $\pi \rightarrow \pi^*(\text{bhq})$].

3.4. Luminescence properties

Detailed experimental data of the emission properties of complexes **1–3** in the solid state are collected in Table 3 and theoretical investigations were performed to explain the corresponding behaviours of the studied complexes (see below). These complexes in the solid state (powder form) at 298 K are emissive upon photoexcitation (see Fig. 6). All complexes with bhq cyclometalated ligands are shown to exhibit a structured profile emission band involving a main peak, a vibronic progression, and a shoulder and these characteristics indicate that in all cases, the emissions arise from a triplet excited state essentially centered on

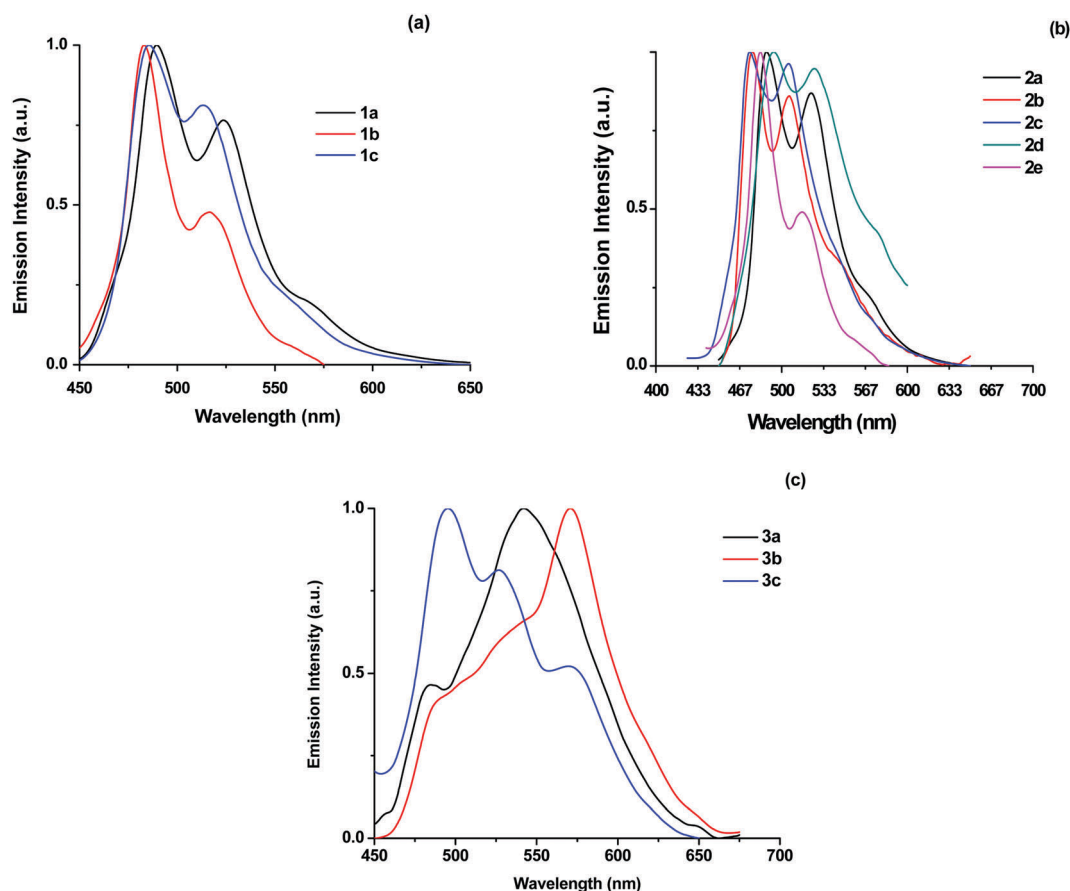


Fig. 6 Luminescence spectra of **1** (a), **2** (b) and **3** (c) in the solid state at 298 K.

Table 4 TD-DFT calculated transitions of the lowest-lying wavelengths and main components of the singlet and triplet excited states of typical complexes **1c**, **2b** and **3b**

Complex	State	Configuration (percentage contribution)	$\lambda_{\text{calc.}}[\text{exp}]/\text{nm}$	Main character
1c	Singlet	HOMO-1 \rightarrow LUMO (83) HOMO \rightarrow LUMO (12)	383[405]	MLCT/LC/LLCT
	Triplet	LSOMO \rightarrow HSOMO (66)	644[560]	MLCT/LC
2b	Singlet	HOMO \rightarrow LUMO (93)	381[414]	MLCT/LC
	Triplet	LSOMO \rightarrow HSOMO (71) LSOMO-3 \rightarrow HSOMO (12)	640[545]	MLCT/LC
3b	Singlet	HOMO \rightarrow LUMO (96)	394[413]	MLCT/LC/LLCT
	Triplet	LSOMO \rightarrow HSOMO (60) LSOMO-1 \rightarrow HSOMO (23)	628[570]	MLCT/LC/LLCT

the bhq ligands (^3LC) involving a mild degree of MLCT admixture.³⁰ As such, comparable patterns were observed in the emission spectra of all our cyclometalated organoplatinum(II) complexes (Fig. 6) giving rise to almost similar emissions and lifetimes in the microsecond range. Although varying the ancillary ligands in the studied cyclometalated organoplatinum(II) complexes (*i.e.* phosphines, anionic, and aryls) shows an effect on the shape and energy of the emission bands, they have an influence on the emission intensities at room temperature. Solid state absolute quantum yields of the complexes $[\text{Pt}(\text{Ph})(\text{bhq})(\text{PPh}_2\text{Me})]$, **2a**, and $[\text{Pt}(p\text{-MeC}_6\text{H}_4)(\text{bhq})(\text{PPhMe}_2)]$, **1c**, being respectively 0.146 and 0.110, are much higher than those observed for the other cyclometalated organoplatinum(II) complexes (the quantum yields for complexes **1a**, **2b**, **2c**, **2d**, **2e**, **3a**, **3b**, and **3c** are measured to be 0.05, 0.021, 0.026, 0.008, 0.030, 0.013, 0.018, and 0.012, respectively).

In the normalized emission spectra of the cyclometalated organoplatinum(II) complexes **1** in the solid state at room temperature (see Fig. 6a), the λ_{em} for the main peaks, vibronic progression peaks, and shoulders appear at about 485 nm, 520 nm, and 560 nm, respectively. The lowest-energy maxima are marginally shifted to lower energies as **1c** (having PPhMe_2 ligand) < **1b** (having PPh_2Me ligand) < **1a** (having PPh_3 ligand). As we progress from **1c** to **1a**, the number of Ph groups on the related phosphine ligand increases and this is expected to decrease the MLCT contribution. This is compensated by the reverse behavior of the LLCT and the above trend is finally obtained.

As can be observed in Fig. 6b, the cyclometalated organoplatinum(II) complexes $[\text{Pt}(p\text{-XC}_6\text{H}_4)(\text{bhq})(\text{PPh}_2\text{Me})]$, **2**, are luminescent in the solid state with λ_{em} between 474 and 494 nm with a tail to lower energies, giving rise to emission bands that are very similar in shape and energy to those found for the **1** isomers. The lowest-energy maxima are dependent on X and are located at 545 nm (for **2b** with X = F) and 577 nm (for **2d** with X = OMe) and the results are consistent with OMe being an electron donor to the Ar ligand (as compared with F having electron withdrawing ability) making the metallic center richer and thus increasing the MLCT contribution; as such the contribution from LLCT is also increased. The lowest-energy maxima for the other complexes with X being H (**2a**), ^tBu (**2c**), and Me (**2e**) are situated in between the **2b** and **2d** extremes.

Solid state emission spectra of the cyclometalated organoplatinum(II) complexes $[\text{Pt}(\text{bhq})\text{X}(\text{PPh}_2\text{Me})]$, **3**, at 298 K have

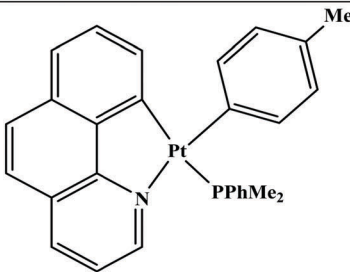
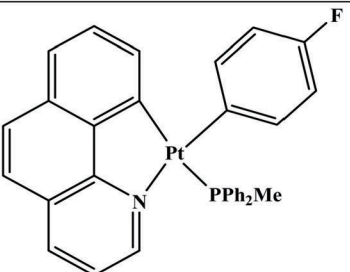
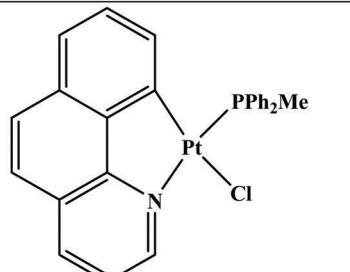
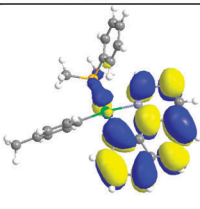
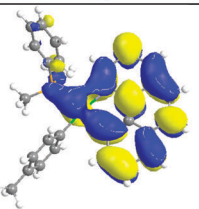
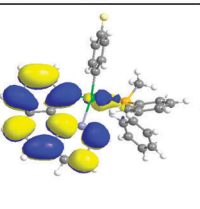
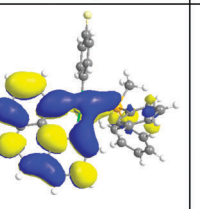
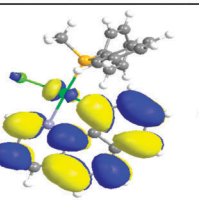
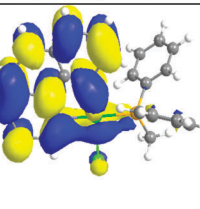
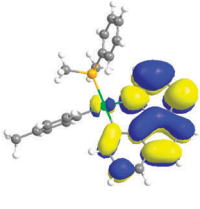
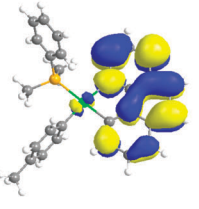
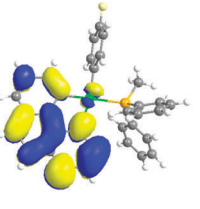
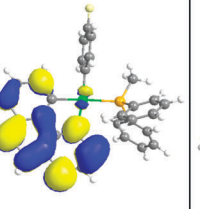
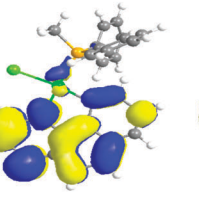
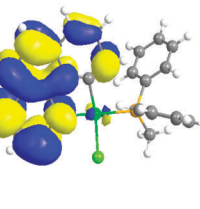
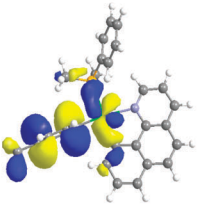
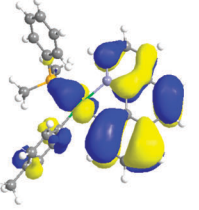
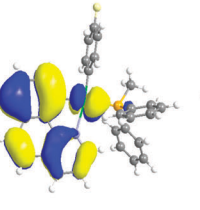
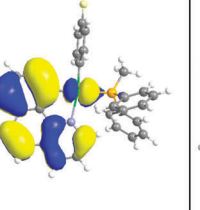
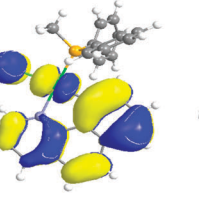
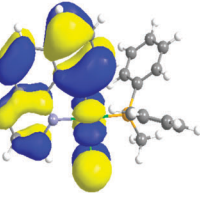
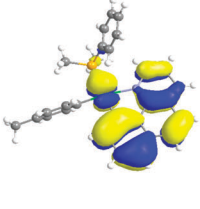
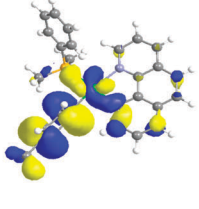
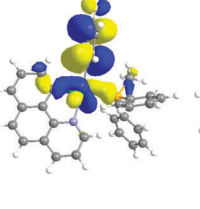
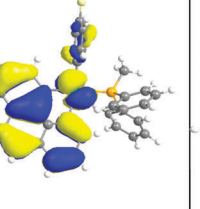
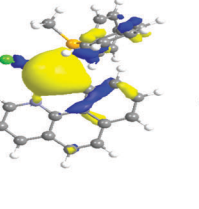
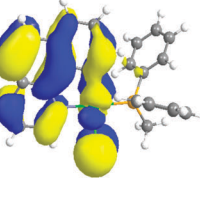
also been recorded (see Fig. 6c) showing that each emission is dependent on the contributions from different transitions (see Tables S32, S36, and S40, ESI†). Notice that the transition admixtures for the tails of the lowest-energy maxima for complexes **3b** (X = Cl) and **3c** (X = I) are MLCT/LC/LLCT, while for complex **3a** (X = CF_3CO_2), probably with the electron withdrawing CF_3 group preventing donation of the lone pair of the O atom connected to the metal center, the related transition admixture is MLCT/LC with no contribution from LLCT, showing a rather significant blue shift as compared with **3a** and **3b**.

The lifetime values for all the cyclometalated organoplatinum(II) complexes studied in the present work (see Table 3) are in the microsecond domain, showing a triplet excited state with phosphorescence character.

3.5. Computational study

Density functional theory (DFT) and time-dependent TD-DFT calculations were performed for all the cyclometalated organoplatinum(II) complexes. The structures were fully optimized and the resulting structures are presented in the Supporting Information. As can be observed in Tables S41–S43 (ESI†), the calculated bond distances and angles are in good agreement with the values obtained from the X-ray crystal structure determination. The negligible differences between the experimental and calculated bond lengths and angles are due to the fact that the computations were performed in the gas phase, while the X-ray data were obtained in the solid phase. To investigate the absorption properties of the cyclometalated organoplatinum(II) complexes, TD-DFT calculations were performed at the B3LYP level of density functional theory. Excitation energies at the ground-state geometries were calculated by TD-DFT in CH_2Cl_2 solution and the gas phase. The data for selected singlet and triplet excitations are given in the Supporting Information and for typical complexes **1c**, **2b** and **3b** are given in Tables 4 and 5. The predicted singlet excitation energies and oscillator strengths are in compliance with the experimental absorption spectra in all the cases. The lowest-energy singlet transition with a significant oscillator strength in all of the cyclometalated organoplatinum(II) complexes is a primarily ligand-centered, LC, (bhq) transition with small contribution of MLCT character, which matches with the experimental absorption between 403 and 417 nm. The lowest singlet excited states in the cyclometalated organoplatinum(II) complex series of $[\text{Pt}(p\text{-MeC}_6\text{H}_4)(\text{bhq})(\text{L})]$, **1**, are derived from the HOMO \rightarrow LUMO and HOMO-1 \rightarrow LUMO

Table 5 Molecular orbital plots for computed S₁ and T₁ states of the typical complexes **1c**, **2b** and **3b**

Complex 1c		Complex 2b		Complex 3b	
					
S ₁	T ₁	S ₁	T ₁	S ₁	T ₁
					
LUMO + 1	HSOMO + 1	LUMO + 1	HSOMO + 1	LUMO + 1	HSOMO + 1
					
LUMO	HSOMO	LUMO	HSOMO	LUMO	HSOMO
					
HOMO	LSOMO	HOMO	LSOMO	HOMO	LSOMO
					
HOMO - 1	LSOMO - 1	HOMO - 1	LSOMO - 1	HOMO - 1	LSOMO - 1

transitions. The $S_0 \rightarrow S_1$ transition originates from the mixed LC/MLCT/LLCT (L = bhq and *p*-tolyl, M = Pt) transitions. The calculated charge on the Pt atom is negative for [Pt(*p*-MeC₆H₄)(bhq)(PPh₃)], **1a**, (−0.001) in comparison with the positive charge in the other two (0.007 and 0.026 for **1b** and **1c** derivatives respectively) that can be attributed to the number of phenyl groups in the phosphine ligands. The lowest-energy

transition in the cyclometalated organoplatinum(II) complex series of [Pt(*p*-XC₆H₄)(bhq)(PPh₂Me)], **2**, corresponds to the mixed LC/MLCT [$\pi(\text{bhq})/\text{d}\sigma(\text{Pt}) \rightarrow \pi^*(\text{bhq})$]. In the case of **2d**, the lowest energy transition is calculated to be the mixed LLCT/MLCT [$(p\text{-MeOC}_6\text{H}_4)/\text{d}\sigma(\text{Pt}) \rightarrow \pi^*(\text{bhq})$] transitions. In comparison with **2a** with the cyclometalated phenyl group, complex **2b** bearing the 4-fluorophenyl group reveals an ~12 nm

hypsochromic shift in the emission peak wavelength and can qualitatively be rationalized by a decrease in π MO energy level due to the stronger electron-withdrawing character of the fluorine atom at a para position. For the cyclometalated organoplatinum(II) complex series of $[\text{Pt}(\text{bhq})\text{X}(\text{PPh}_2\text{Me})]$, **3**, the lowest-energy transition is related to the mixed LC/MLCT $[\pi(\text{bhq})/\text{d}\sigma(\text{Pt}) \rightarrow \pi^*(\text{bhq})]$ transitions with an additional LLCT character in **3c** ($\text{X} = \text{I}$) $[\text{p}(\text{I}) \rightarrow \pi^*(\text{bhq})]$ which is responsible for the long tail observed in the experimental absorption spectrum of **3c**; more intense bands at higher energies in **3** complexes seem to be related to the mixed LC/LLCT/MLCT $[\pi(\text{bhq})/\text{p}(\text{X})/\text{d}(\text{Pt}) \rightarrow \pi^*(\text{bhq})]$ transitions. Although in **3a** and **3b**, there are negligible contributions from $\text{p}(\text{CF}_3\text{CO}_2)$ and $\text{p}(\text{Cl})$ orbitals, the contributions from $\text{p}(\text{I})$ orbitals in **3c** are appreciably higher and almost 50% of the HOMO–1 is iodine p-orbitals.

The TD–DFT results show $^3\text{LC}(\text{bhq})$ character as the lowest triplet (T_1) in the calculated cyclometalated organoplatinum(II) complexes, with different contributions of MLCT or LLCT character, agreeing with the obtained experimental emissions. It is noteworthy that a relatively high amount of MLCT character is found in the first three triplets of all of the complexes. The lowest-energy triplet in the cyclometalated organoplatinum(II) complex series of $[\text{Pt}(p\text{-MeC}_6\text{H}_4)(\text{bhq})(\text{L})]$, **1**, the **1a** and **1b** complexes have a mixed LLCT/MLCT/LC character $[\text{d}\sigma(\text{Pt})/\pi(\text{bhq})/\pi(p\text{-tol}) \rightarrow \pi^*(\text{bhq})]$. However, for complex **1c**, the LLCT character $[\pi(p\text{-tol}) \rightarrow \pi^*(\text{bhq})]$ is not present in the above-mentioned transitions. The cyclometalated organoplatinum(II) complex series of $[\text{Pt}(p\text{-XC}_6\text{H}_4)(\text{bhq})(\text{PPh}_2\text{Me})]$, **2**, possess LC/MLCT $[\text{d}\sigma(\text{Pt})/\pi(\text{bhq}) \rightarrow \pi^*(\text{bhq})]$ character in their emissive states. The small contribution of LLCT character $[\pi(p\text{-XC}_6\text{H}_4)/\pi(\text{bhq}) \rightarrow \pi^*(\text{bhq})]$ is observed for the **2a** ($\text{Ar} = \text{C}_6\text{H}_5$) and **2e** ($\text{Ar} = p\text{-MeC}_6\text{H}_5$) complexes lying relatively close to the lowest triplet. However, for complexes **2b–2d** there is no observable ligand to ligand charge transfer in their lowest-energy triplet state. The presence of thermally accessible low-lying LLCT $[\text{p}(\text{X}) \rightarrow \pi^*(\text{bhq})]$ states, ($\text{X} = \text{CF}_3\text{CO}_2$, Cl , I) in the cyclometalated organoplatinum(II) complex series of $[\text{Pt}(\text{bhq})\text{X}(\text{PPh}_2\text{Me})]$, **3**, indicates that the population of LLCT character (excitation energies 2.63, 2.7 and 1.9 eV for **3a**, **3b** and **3c** respectively) could be responsible for the low quantum yield values caused by nonradiative deactivation at 298 K. In this series, complex **3c** has the lowest-lying LLCT state and consequently the lowest quantum yield. In contrast, similar states are significantly higher in energy for complex **2a** (3.36 eV), exhibiting its more efficient emissions at 298 K.

4. Conclusions

Three series of cyclometalated organoplatinum(II) complexes were synthesized and fully characterized using multinuclear NMR spectroscopy and X-ray crystallography. By systematically modifying different kinds of ancillary ligands and changing the substituents on them, the effect of each part on their luminescence properties was studied.

The UV-vis transitions of the studied complexes are comparable to those reported for the complexes $[\text{Pt}(p\text{-MeC}_6\text{H}_4)(\text{bhq})(\text{SMe}_2)]$,

showing that ^1LC transitions within the bhq cyclometalated ligand ($\pi\text{--}\pi^*$) are dominating. The lowest-energy band in the cyclometalated organoplatinum(II) complexes of series $[\text{Pt}(p\text{-MeC}_6\text{H}_4)(\text{bhq})(\text{L})]$, **1**, comprises LLCT, MLCT and LC transitions that show slight dependence on the nature of the phosphine ligands. The complexes series $[\text{Pt}(p\text{-XC}_6\text{H}_4)(\text{bhq})(\text{PPh}_2\text{Me})]$, **2**, have MLCT and LC transitions, although complexes **2c** and **2e** have an additional LLCT transition. The maxima of the complexes series $[\text{Pt}(\text{bhq})\text{X}(\text{PPh}_2\text{Me})]$, **3**, show minor changes with the variation of anionic ligands indicating that they arise mostly from $^1\text{LC}(\text{bhq})$ transitions, although the slopes of the lowest-energy maxima slightly shift to lower energies according to the π -donating ability of the X ligands.

Investigations of the photophysical properties of the three series of cyclometalated organoplatinum(II) complexes indicated that these complexes are emissive in the solid state with the lifetimes being on the order of μs . Varying the ancillary ligands in the studied cycloplatinated complexes (*i.e.* phosphines, anionic, and aryls) shows an effect on the shape or energy of the emission bands; also they have an influence on the emission intensities at room temperature. The structured bands in the normalized emission spectra of the cyclometalated organoplatinum(II) complexes indicate the presence of a large amount of ligand-centered LC/MLCT ($\text{L} = \text{bhq}$) character in the emissive excited state, confirming that the emissions originate from the cyclometalated moiety $\text{Pt}(\text{C}^{\wedge}\text{N})$. Furthermore, our calculations suggest that transitions in the cyclometalated organoplatinum(II) complexes are a function of the aromatic ligand, degree of aromaticity, and attached electron donor/acceptor groups.

Conflicts of interest

There are no conflicts to declare.

Acknowledgements

Financial support from Shiraz University is gratefully acknowledged. Also MGH is thankful for the financial support of the Iran National Science Foundation (grant no. 94010886) and the support of Shahid Beheshti University Research Councils.

References

- 1 S. W. Botchway, M. Charnley, J. W. Haycock, A. W. Parker, D. L. Rochester, J. A. Weinstein and J. G. Williams, *Proc. Natl. Acad. Sci. U. S. A.*, 2008, **105**, 16071–16076.
- 2 E. Baggaley, J. A. Weinstein and J. G. Williams, *Coord. Chem. Rev.*, 2012, **256**, 1762–1785.
- 3 X. Mou, Y. Wu, S. Liu, M. Shi, X. Liu, C. Wang, S. Sun, Q. Zhao, X. Zhou and W. Huang, *J. Mater. Chem.*, 2011, **21**, 13951–13962.
- 4 M. Jamshidi, M. Babaghasabha, H. R. Shahsavari and S. M. Nabavizadeh, *Dalton Trans.*, 2017, **46**, 15919–15927.
- 5 M. Jamshidi, S. M. Nabavizadeh, H. Sepehrpour, F. N. Hosseini, R. Kia and M. Rashidi, *J. Lumin.*, 2016, **179**, 222–229.

- 6 M. Jamshidi, S. M. Nabavizadeh, H. R. Shahsavari and M. Rashidi, *RSC Adv.*, 2015, **5**, 57581–57591.
- 7 C. A. Craig and R. J. Watts, *Inorg. Chem.*, 1989, **28**, 309–313.
- 8 H. Yersin, P. Huber and H. Wiedenhofer, *Coord. Chem. Rev.*, 1994, **132**, 35–42.
- 9 L. Chassot and A. Von Zelewsky, *Inorg. Chem.*, 1987, **26**, 2814–2818.
- 10 S. Jamali, S. M. Nabavizadeh and M. Rashidi, *Inorg. Chem.*, 2008, **47**, 5441–5452.
- 11 A. Zucca, G. L. Petretto, S. Stoccoro, M. A. Cinellu, M. Manassero, C. Manassero and G. Minghetti, *Organometallics*, 2009, **28**, 2150–2159.
- 12 J. S. Owen, J. A. Labinger and J. E. Bercaw, *J. Am. Chem. Soc.*, 2004, **126**, 8247–8255.
- 13 S. M. Nabavizadeh, M. G. Haghighi, A. R. Esmailbeig, F. Raoof, Z. Mandegani, S. Jamali, M. Rashidi and R. J. Puddephatt, *Organometallics*, 2010, **29**, 4893–4899.
- 14 M. G. Haghighi, S. M. Nabavizadeh, M. Rashidi and M. Kubicki, *Dalton Trans.*, 2013, **42**, 13369–13380.
- 15 A. Esmailbeig, H. Samouei, S. Abedanzadeh and Z. Amirghofran, *J. Organomet. Chem.*, 2011, **696**, 3135–3142.
- 16 B. Shafaatian, A. Akbari, S. M. Nabavizadeh, F. W. Heinemann and M. Rashidi, *Dalton Trans.*, 2007, 4715–4725, DOI: 10.1039/B708769A.
- 17 F. Julia, M.-D. García-Legaz, D. Bautista and P. González-Herrero, *Inorg. Chem.*, 2016, **55**, 7647–7660.
- 18 M. J. Frisch, N. Rega, G. A. Petersson, G. W. Trucks, H. Nakatsuji, M. Hada, M. Ehara, K. Toyota, R. Fukuda, J. Hasegawa, M. Ishida, J. C. Burant, T. Nakajima, Y. Honda, O. Kitao, H. B. Schlegel, H. Nakai, M. Klene, X. Li, J. E. Knox, H. P. Hratchian, J. B. Cross, J. M. Millam, V. Bakken, C. Adamo, J. Jaramillo, R. Gomperts, G. E. Scuseria, R. E. Stratmann, O. Yazyev, A. J. Austin, R. Cammi, C. Pomelli, S. S. Iyengar, J. W. Ochterski, P. Y. Ayala, K. Morokuma, G. A. Voth, P. Salvador, M. A. Robb, J. J. Dannenberg, V. G. Zakrzewski, S. Dapprich, A. D. Daniels, J. Tomasi, M. C. Strain, O. Farkas, D. K. Malick, A. D. Rabuck, K. Raghavachari, J. B. Foresman, J. R. Cheeseman, J. V. Ortiz, Q. Cui, A. G. Baboul, V. Barone, S. Clifford, J. Cioslowski, B. B. Stefanov, G. Liu, A. Liashenko, P. Piskorz, I. Komaromi, J. A. Montgomery Jr, R. L. Martin, D. J. Fox, B. Mennucci, T. Keith, M. A. Al-Laham, C. Y. Peng, A. Nanayakkara, M. Challacombe, P. M. W. Gill, B. Johnson, W. Chen, T. Vreven, M. W. Wong, M. Cossi, C. Gonzalez, J. A. Pople, K. N. Kudin and G. Scalmani, *Gaussian 03, Revision C.02*, 2004.
- 19 P. J. Hay and W. R. Wadt, *J. Chem. Phys.*, 1985, **82**, 270–283.
- 20 M. Cossi, G. Scalmani, N. Rega and V. Barone, *J. Chem. Phys.*, 2002, **117**, 43–54.
- 21 V. Barone, M. Cossi and J. Tomasi, *J. Chem. Phys.*, 1997, **107**, 3210–3221.
- 22 P. S. Hanley and J. F. Hartwig, *J. Am. Chem. Soc.*, 2011, **133**, 15661–15673.
- 23 S. Bhargava, K. Kitadai, T. Masashi, D. W. Drumm, S. P. Russo, V. W.-W. Yam, T. K.-M. Lee, J. Wagler and N. Mirzadeh, *Dalton Trans.*, 2012, **41**, 4789–4798.
- 24 E. Glendening, A. Reed, J. Carpenter and F. Weinhold, *NBO Version 3.1*, Gaussian, Inc., Wallingford, CT, 2004, included in Gaussian03.
- 25 *Rigaku Oxford Diffraction, CrysAlisPro, Version 1.171.38.37b*, 2015.
- 26 L. Palatinus and G. Chapuis, *J. Appl. Crystallogr.*, 2007, **40**, 786–790.
- 27 V. Petříček, M. Dušek and L. Palatinus, *Z. Kristallogr. – Cryst. Mater.*, 2014, **229**, 345–352.
- 28 M. G. Haghighi, M. Rashidi, S. M. Nabavizadeh, S. Jamali and R. J. Puddephatt, *Dalton Trans.*, 2010, **39**, 11396–11402.
- 29 S. M. Nabavizadeh, H. R. Shahsavari, M. Namdar and M. Rashidi, *J. Organomet. Chem.*, 2011, **696**, 3564–3571.
- 30 R. B. Aghakhanpour, S. M. Nabavizadeh, M. Rashidi and M. Kubicki, *Dalton Trans.*, 2015, **44**, 15829–15842.